5196

Novel Humanized CD36 Mouse Model for Therapeutic Studies

Linlin Wang[1], Chang Liu[1], Rebecca Soto[2], Chengzhang Shang[1], Qingcong Lin[2]

[1] Biocytogen (Pharmaceuticals) Beijing Co., Beijing, China; [2] Biocytogen Boston Corporation, Wakefield, MA, USA

biocytogen.com | info@biocytogen.com

ABSTRACT

Activation of oncogenic signaling pathways can be mediated by various transporters on tumor cells that facilitate trafficking of lipids. CD36 has been identified as a fatty acid transporter and participates in tumor growth and drug resistance. To explore potential therapeutic strategies targeting CD36, we generated a human CD36 knockout/knock-in in situ (B-hCD36) mouse model to evaluate the efficacy of anti-human CD36 antibodies. We first confirmed human CD36 gene and protein expression in B-hCD36 mice by RT-PCR and flow cytometry, respectively. We next observed that the overall development, differentiation, or distribution of splenic, blood and lymph node immune cells were similar between wild-type C57BL/6 and B-hCD36 mice. Lastly, in vivo efficacy studies using anti-human CD36 antibodies alone or in combination with anti-mouse PD-1 antibodies, were effective in controlling MC38 tumor growth in B-hCD36 mice. Our data demonstrates that B-hCD36 mice are a powerful preclinical model for in vivo efficacy evaluation of anti-human CD36 antibodies.

Human *CD36* Gene Expression Analysis in B-hCD36 Mice

Species-specific *CD36* gene expression analysis in wild-type and humanized B-hCD36 mice by RT-PCR. Murine *Cd36* mRNA was detected in lung tissue isolated from wild-type C57BL/6$^{(+/+)}$ mice, while human *CD36* mRNA was detected in homozygous B-hCD36$^{(H/H)}$ mice.

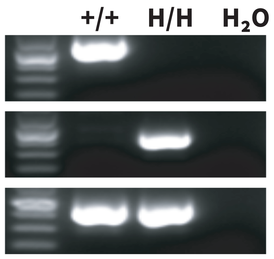

Human CD36 Protein Expression Analysis in B-hCD36 Mice

Species-specific CD36 protein expression analysis in wild-type and humanized B-hCD36 mice. Peritoneal exudate macrophages were isolated from wild-type C57BL/6$^{(+/+)}$ and homozygous B-hCD36$^{(H/H)}$ mice and analyzed by flow cytometry using species-specific anti-CD36 antibodies. Murine CD36 protein was detected in wild-type mice, while human CD36 protein was detected in B-hCD36 mice.

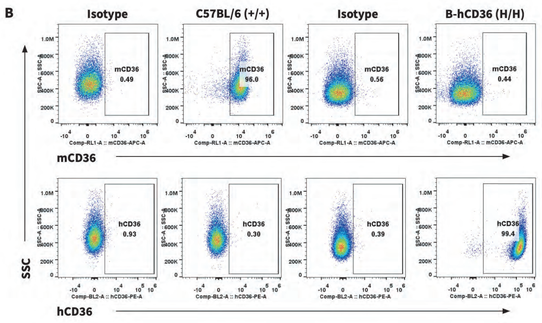

Normal Blood and Liver Profile in B-hCD36 Mice

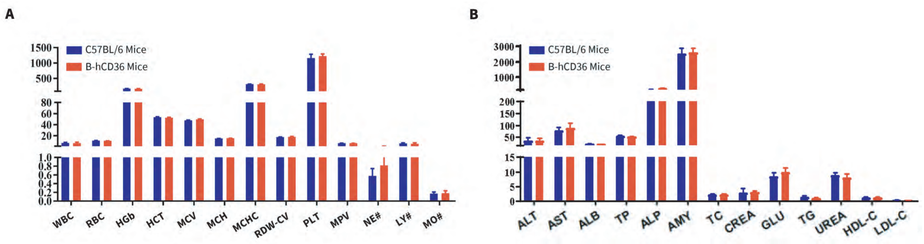

Blood routine tests and chemistry assessed in wild-type and humanized B-hCD36 mice. Blood from wild-type C57BL/6 and humanized B-hCD36 mice (female, n=8, 6-8-week-old) was collected and analyzed. (A) Complete blood count. (B) Blood chemistry. Measurements in B-hCD36 mice were comparable to wild-type C57BL/6 mice, indicating that humanization does not change blood cell composition or the health of related tissues, such as liver. Values are expressed as mean ± SEM.

Immune Cell Analysis in Humanized B-hCD36 Mice

Immune cell analysis in wild-type and humanized B-hCD36 mice. Spleen, lymph node, and blood-derived immune cells were isolated from wild-type C57BL/6$^{(+/+)}$ and homozygous B-hCD36$^{(H/H)}$ mice and analyzed by flow cytometry. Percent of immune cells in B-hCD36 mice were similar to those in wild-type mice, demonstrating that CD36 humanization does not change the overall development, differentiation, or distribution of these immune cells in B-hCD36 mice. Values are expressed as mean ± SEM.

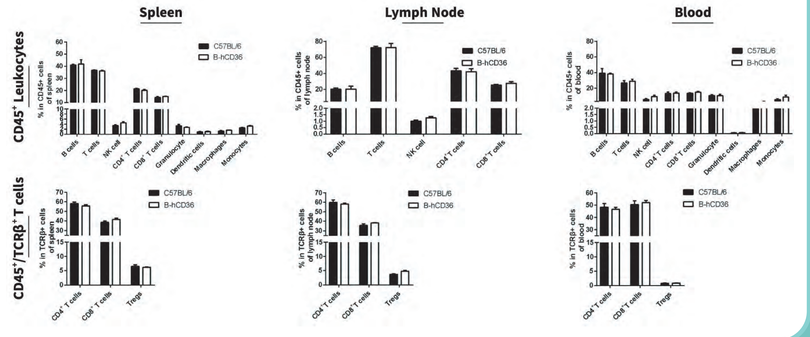

In vivo Efficacy of an Anti-CD36 Antibody

Anti-tumor activity of an anti-CD36 antibody in humanized B-hCD36 mice. Murine colon cancer MC38 cells were subcutaneously implanted into homozygous B-hCD36 mice (female, 8-week-old, n=6). Mice were grouped and treated with different doses of an anti-CD36 antibody (in house) when the tumor volume reached approximately 100 mm^3. (A) The anti-CD36 antibody controlled MC38 tumor growth in B-hCD36 mice, (B) without negatively impacting body weight changes. Values are expressed as mean ± SEM.

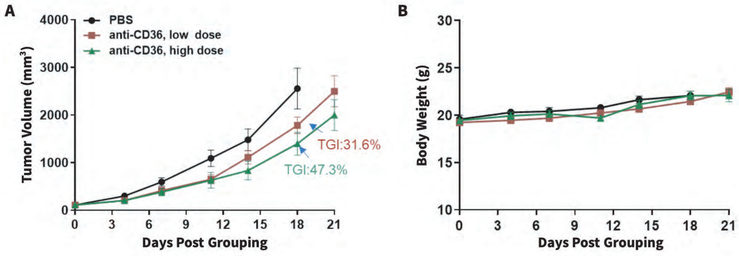

Combination Therapy Using Anti-human CD36 and Anti-mouse PD-1 Antibodies

Anti-tumor activity of an anti-mouse PD-1 antibody combined with an anti-human CD36 antibody in B-hCD36 mice. Murine colon cancer MC38 cells were subcutaneously implanted into homozygous B-hCD26 mice (female, 7-week-old, n=5). Mice were grouped and treated with antibodies at schedules and doses as indicated in panel A when the tumor volume reached approximately 60 mm^3. (A) Anti-mPD-1 antibody combined with an anti-hCD36 antibody inhibited MC38 tumor growth in B-hCD36 mice, (B) without negatively impacting body weight changes. This demonstrates that B-hCD36 mice are a powerful preclinical model for in vivo evaluation of anti-CD36 antibodies.
*Antibodies were provided by the client. Values are expressed as mean ± SEM.

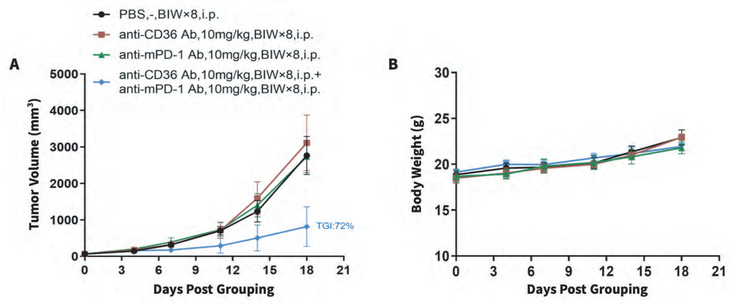

CONCLUSIONS

mRNA expression analysis:
Mouse *Cd36* mRNA was detected in lung tissue isolated from wild-type mice, while human *CD36* mRNA was detected in homozygous B-hCD36 mice.

Protein expression analysis:
Human CD36 protein was detected in homozygous B-hCD36 mice, but not in wild-type mice.

Immune cell analysis:
CD36 humanization does not change the overall development, differentiation or distribution of spleen, lymph node, and blood immune cells in B-hCD36 mice.

***In vivo* efficacy of anti-CD36 antibodies:**
Anti-CD36 mono- and combination therapy controlled MC38 tumor growth in B-hCD36 mice.

3286

B-hCD94/hNKG2A Mice Provide a Preclinical Tool for Evaluating Therapeutic Antibodies Targeting Human NKG2A

BIOCYTOGEN

BIOMICE

Chengzhang Shang[1], Fang He[1], Mari Kuraguchi[2], Jing Zhang[1], Qingcong Lin[2]

[1] Biocytogen (Pharmaceuticals) Beijing Co., Beijing, China; [2] Biocytogen Boston Corporation, Wakefield, MA, USA

biocytogen.com | info@biocytogen.com

ABSTRACT

The immune cell checkpoint NKG2A and its coreceptor, CD94, are expressed by many circulating NK cells and by a subset of CD8 T cells in tumors. When CD94/NKG2A recognizes the HLA-E-peptide complex, the protein tyrosine phosphatase SHP-1 is recruited to the signaling synapse, resulting in the delivery of inhibitory signals to the effector cells and inhibition of their immune activities. In preclinical mouse models, blocking antibodies against NKG2A restores the reactivity of these effector cells, resulting in better suppression of tumor growth. Thus, NKG2A targeting is currently being evaluated in the clinic to evaluate tumor cell killing. To evaluate the *in vivo* efficacy of anti-NKG2A in mice, we successfully generated a humanized CD94/NKG2A double knock-in mouse strain (B-hCD94/hNKG2A mice), in which the mouse *Cd94* and *Nkg2a* genes are replaced by the corresponding human *CD94* and *NKG2A* genes *in situ in cis*, respectively. Human CD94 and NKG2A mRNA and proteins were exclusively detectable by flow cytometry in homozygous humanized mice, confirming successful generation of the model. This model was used to demonstrate *in vivo* efficacy of monalizumab analog in suppressing the growth of MC38 tumor cells expressing human HLA-E (B-hHLA-E MC38). Furthermore, dual blockade by monalizumab and anti-PD-L1 further suppressed B-hHLA-E MC38 tumor growth. Together, these data indicate that this double humanized model is an effective tool for evaluating novel anti-human NKG2A therapies and warrants the generation of a quadruple humanized model (B-hPD-1/hPD-L1/hCD94/hNKG2A mice) to further evaluate the synergy of drugs blocking each checkpoint.

CD94 & NKG2A Gene Expression Analysis in Humanized B-hCD94/hNKG2A Mice

Species-specific *CD94* and *NKG2A* gene expression analysis in wild-type and humanized B-hCD94/hNKG2A mice by RT-PCR. Mouse *Cd94* and *Nkg2a* mRNAs were detected in splenocytes isolated from wild-type C57BL/6 (+/+) mice, while human *CD94* and *NKG2A* mRNAs were detected in homozygous B-hCD94/hNKG2A (H/H) mice.

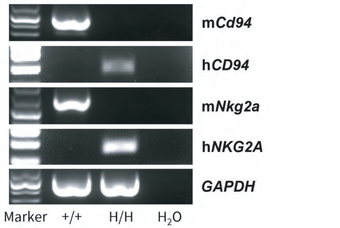

CD94 & NKG2A Protein Expression Analysis in NK Cells

Species-specific CD94 and NKG2A protein expression analysis in wild-type and humanized B-hCD94/hNKG2A mice. Splenocytes were isolated from wild-type C57BL/6 (+/+) and homozygous B-hCD94/hNKG2A (H/H) mice and analyzed by flow cytometry using species-specific anti-CD94 and anti-NKG2A antibodies. Mouse CD94 and NKG2A proteins were detected in wild-type mice, while human CD94 and NKG2A proteins were detected in B-hCD94/hNKG2A mice. (Monalizumab was used to detect human NKG2A protein in wild-type and B-hCD94/hNKG2A mice).

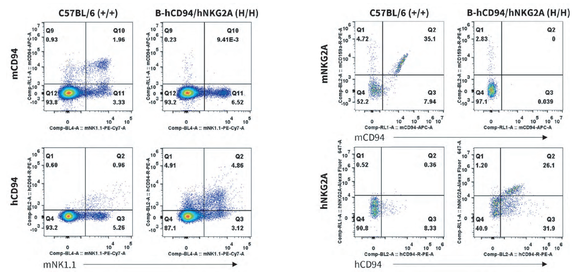

Spleen Immune Cell Analysis in Humanized B-hCD94/hNKG2A Mice

Spleen immune cell analysis in wild-type and humanized B-hCD94/hNKG2A mice. Splenocytes were isolated from wild-type C57BL/6 and humanized B-hCD94/hNKG2A mice (female, n=3, 6-weeks-old) and analyzed by flow cytometry to assess leukocytes. (A) Representative flow cytometry plots gated on single live CD45⁺ cells. (B) Percent of T, B, NK cells, monocytes/macrophages, and DC were similar between B-hCD94/hNKG2A mice and wild-type mice, demonstrating that introduction of hCD94/hNKG2A in place of its mouse counterpart does not change the overall development, differentiation, or distribution of these spleen cell types. Values are expressed as mean ± SEM.

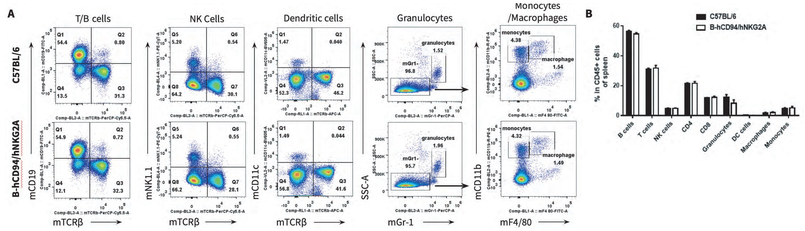

Spleen Immune Cell Analysis in Humanized B-hCD94/hNKG2A Mice (cont'd)

Spleen immune cell analysis in wild-type and humanized B-hCD94/hNKG2A mice. Splenocytes were isolated from wild-type C57BL/6 and humanized B-hCD94/hNKG2A mice (female, n=3, 6 weeks-old) and analyzed by flow cytometry for T cell subsets. (A) Representative flow cytometry plots indicated single live TCRβ^+ T cells were used for further analysis. (B) Percent of CD8$^+$, CD4$^+$, and Treg cells were similar between B-hCD94/hNKG2A and wild-type mice, demonstrating that introduction of hCD94/hNKG2A in place of its mouse counterpart does not change the overall development, differentiation or distribution of these spleen T cell subtypes. Values are expressed as mean ± SEM.

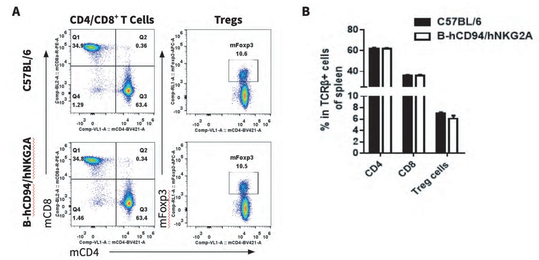

In vivo Efficacy of an Anti-Human NKG2A Antibody in B-hCD94/hNKG2A Mice

Antitumor activity of an anti-human NKG2A antibody in B-hCD94/hNKG2A mice. Murine colon cancer B-hHLA-E MC38 cells were subcutaneously implanted into homozygous B-hCD94/hNKG2A mice (female, 6-7-week-old, n=5). Mice were grouped when tumor volume reached approximately 100 mm^3, and treated with an anti-human NKG2A antibody (Monalizumab, in house) at doses indicated in panel A. (A) Monalizumab inhibited hHLA-E MC38 tumor growth in a dose-dependent manner in B-hCD94/hNKG2A mice. (B) Body weight changes during treatment. B-hCD94/hNKG2A mice provide a powerful preclinical model for *in vivo* evaluation of anti-human NKG2A antibodies. Values are expressed as mean ± SEM.

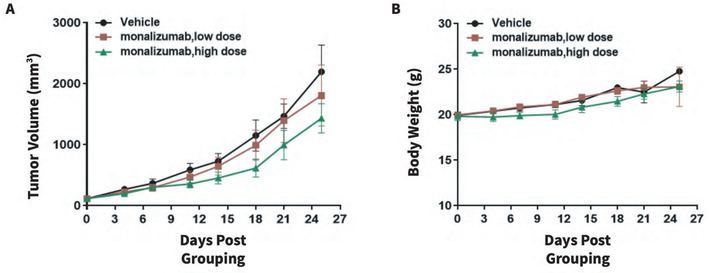

Combination Therapy of Atezolizumab and Monalizumab in B-hCD94/hNKG2A Mice

Antitumor activity of Atezolizumab combined with Monalizumab in humanized B-hCD94/hNKG2A mice. Murine colon cancer B-hHLA-E MC38 cells were subcutaneously implanted into homozygous B-hCD94/hNKG2A mice (female, 6-7-week-old, n=6). Mice were grouped when tumor volume reached approximately 100 mm^3, at which time they were treated with an anti-human NKG2A antibody (Monalizumab, from partner) and/or an anti-human PD-L1 antibody (Atezolizumab, from partner) at schedules indicated in panel A. (A) Monalizumab combined with Atezolizumab inhibited B-hHLA-E MC38 tumor growth in B-hCD94/hNKG2A mice. (B) Body weight changes during treatment. B-hCD94/hNKG2A mice provide a powerful preclinical model for evaluating PD-L1 and NKG2A combination therapy. Values are expressed as mean ± SEM.

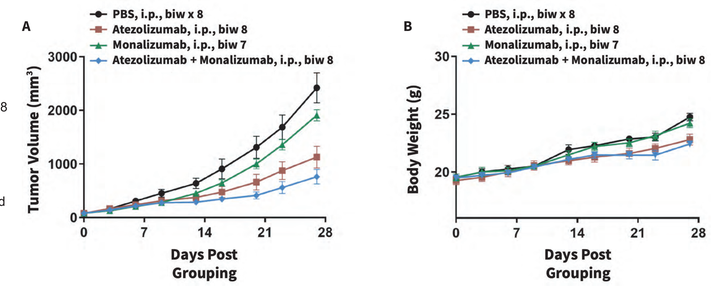

CONCLUSIONS

mRNA expression analysis:
Mouse *Cd94* and *Nkg2a* mRNAs were detected in splenocytes isolated from wild-type mice, while human *CD94* and *NKG2A* mRNAs were detected in homozygous B-hCD94/hNKG2A mice.

Protein expression analysis:
Human CD94 and NKG2A proteins were detected in homozygous B-hCD94/hNKG2A mice, but not in wild-type mice.

Immune cell analysis:
CD94 and NKG2A humanization does not change the overall development, differentiation or distribution of spleen, lymph node (data not shown), and blood (data not shown) immune cells in B-hCD94/hNKG2A mice.

***In vivo* efficacy of an anti-human NKG2A antibody:**
Anti-human NKG2A mono- and combination therapy controlled B-hHLA-E MC38 tumor growth in B-hCD94/hNKG2A mice.

3993

In vivo Efficacy of an Anti-Human IL11RA Antibody in B-hIL11RA Mice With APAP-Induced Liver Damage

BIOCYTOGEN

BIOMICE

Fang He[1], Rufeng Zhang[1], Mari Kuraguchi[2], Lei Zhao[1], Zhaoxue Yu[2]

[1] Biocytogen (Pharmaceuticals) Beijing Co., Beijing, China; [2] Biocytogen Boston Corporation, Wakefield, MA, USA

ABSTRACT

Acetaminophen (N-acetyl-p-aminophenol; APAP) overdose is a common cause of drug-induced acute liver injury, thereby making APAP administration a frequently used experimental model due to its highly reproducible and dose-dependent hepatoxicity. APAP-induced liver injury (AILI) mouse models exhibited upregulated IL11 expression, indicating that targeting IL11 or its cognate receptor, IL11RA, could have therapeutic potential. To evaluate the *in vivo* efficacy of anti-human IL11RA antibodies in AILI mouse models, we first generated a human IL11RA knock-in mouse model (B-hIL11RA), in which human *IL11RA* replaced murine *Il11ra*, in situ. Human IL11RA mRNA and protein levels were detected in B-hIL11RA mice. We next examined whether therapeutic inhibition of IL11 signaling was effective in reducing AILI following administration of an anti-human IL11RA antibody. *In vivo* efficacy data showed that anti-human IL11RA antibody inhibited all aspects of AILI, including hepatocyte death (ALT, AST and TUNEL) and centrilobular necrosis. These data suggest that B-hIL11RA mice are an effective tool for preclinical *in vivo* efficacy evaluation of therapeutic anti-human IL11RA antibodies.

Human IL11RA protein expression analysis in B-hIL11RA mice

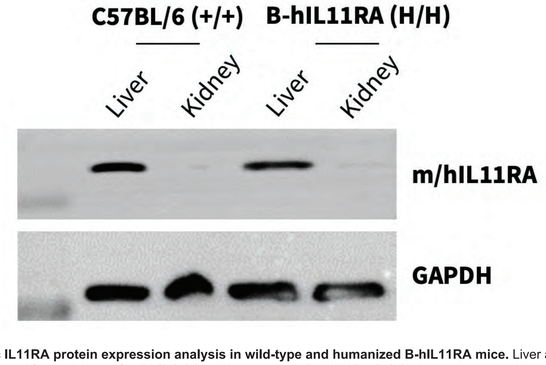

Tissue-specific IL11RA protein expression analysis in wild-type and humanized B-hIL11RA mice. Liver and kidney tissues were isolated from wild-type C57BL/6 (+/+) and homozygous B-hIL11RA (H/H) mice and analyzed by western blot using a cross-reactive anti-m/hIL11RA antibody. IL11RA protein was detected in the liver from wild-type and B-hIL11RA mice but not in kidney.

Reduction in APAP-induced liver damage in B-hIL11RA mice using an anti-human IL11RA antibody

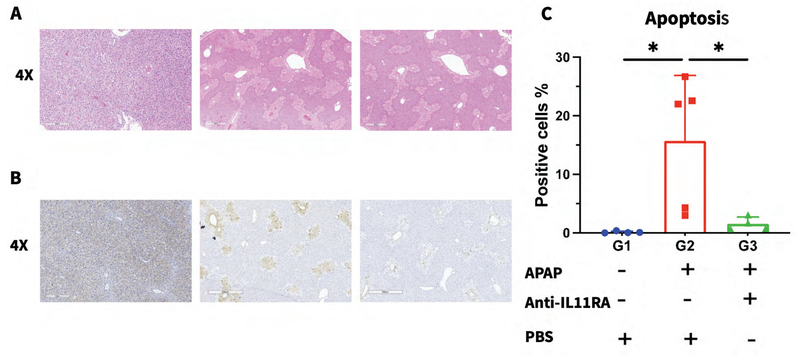

Reduction in APAP-induced liver damage in B-hIL11RA mice using an anti-human IL11RA antibody. (A) Representative liver sections H&E-stained liver images (representative dataset from *n* = 4 or 5 per group). Histology showed typical and extensive necrosis in group G2, which was almost not observed in group G1 and reduced in group G3. (B) Representative TUNEL-stained liver images (representative dataset from *n* = 4 or 5 per group). (C) Statistical analysis of TUNEL positive cells (% of total cells). Significance was determined by Mann-Whitney test. Values are expressed as mean ± SD. *p<0.05.

Human *IL11RA* mRNA expression analysis in B-hIL11RA mice

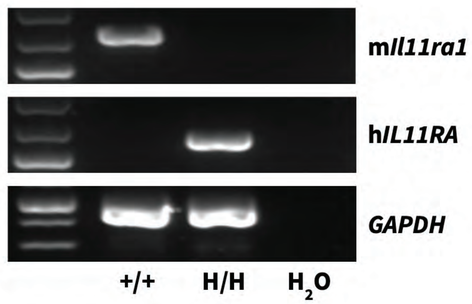

Species-specific *IL11RA* gene expression analysis in wild-type and B-hIL11RA mice by RT-PCR. Murine *Il11ra1* mRNA was detected in liver tissue isolated from wild-type C57BL/6 (+/+) mice, while human *IL11RA* mRNA was detected in homozygous B-hIL11RA (H/H) mice.

In vivo efficacy of an anti-human IL11RA antibody with APAP-induced liver damage in B-hIL11RA mice

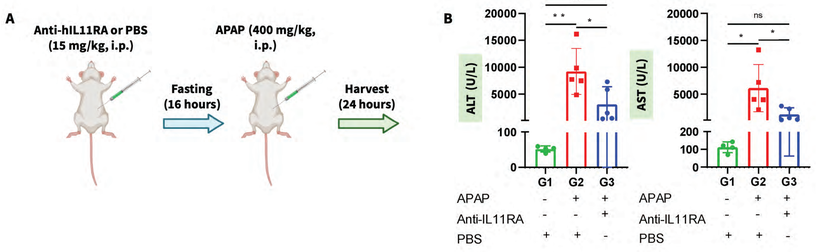

Reduction in APAP-induced liver damage with an anti-human IL11RA antibody in male B-hIL11RA mice. (A) Schematic showing therapeutic dosing of APAP-injured B-hIL11RA mice. B-hIL11RA mice (male, 8 weeks, n=4 - 5) treated with PBS or an anti-hIL11RA antibody (in house, 15 mg/kg) were fasted overnight and exposed to APAP (400 mg/kg) for 24 h. Blood samples were collected for analysis. (B) Serum ALT and AST levels decreased in mice treated with an anti-hIL11RA antibody compared to APAP alone. Significance was determined by one-way ANOVA with Tukey's multiple comparison test. Values are expressed as mean ± SD. *p<0.05, **p<0.01 .

CONCLUSIONS

mRNA expression analysis:
Murine *Il11ra1* mRNA was detected in liver tissue isolated from wild-type C57BL/6 (+/+) mice, while human *IL11RA* mRNA was detected in homozygous B-hIL11RA (H/H) mice.

Protein expression analysis:
IL11RA protein was detected in the liver from wild-type and B-hIL11RA mice.

***In vivo* efficacy:**
Anti-human IL11RA antibody alleviated APAP-induced liver damage in humanized B-hIL11RA mice.

5178

Humanized OX40/OX40L Mice as a Tool for Evaluating Novel Therapeutics

BIOCYTOGEN

BIOMICE

Chonghui Liu[1], Jiawei Yao[1], Xiaofei Zhou[1], James Jin[2], Zan Zhang[1]

[1] Biocytogen (Pharmaceuticals) Beijing Co., Beijing, China; [2] Biocytogen Boston Corporation, Wakefield, MA, USA

ABSTRACT

The use of immune-competent mouse models that express target human genes provide a promising preclinical platform aimed at developing novel immunotherapies. Emerging immunotherapies include targeting OX40 and OX40 ligand (OX40L), which can lead to enhanced T cell activation, proliferation, and effector function. Blocking the OX40/OX40L pathway improves autoantigen-specific T cell responses and decreases immunocompetence across several autoimmune diseases. To explore the potential of OX40 and OX40L antibody efficacy studies, we developed double humanized B-hOX40/hOX40L mice by replacing the extracellular domain sequences of murine *Ox40* and *Ox40l* with the corresponding human sequences. We validated human *OX40L* gene expression by RT-PCR and OX40/OX40L protein expression by flow cytometry in B-hOX40/hOX40L mice. Additionally, percentages of splenic, blood, and lymph node immune cells were similar between B-hOX40/hOX40L and wild-type C57BL/6 mice. Altogether, this data demonstrates that B-hOX40/hOX40L mice are suitable for in vivo efficacy studies using anti-human OX40 and OX40L antibodies.

Human *OX40L* gene expression analysis in humanized B-hOX40/hOX40L mice

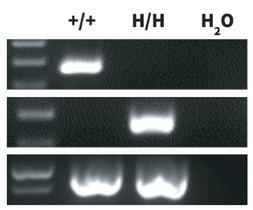

Species-specific *OX40L* gene expression analysis in wild-type and humanized B-hOX40/hOX40L mice by RT-PCR. Murine *Ox40l* mRNA was detected in dendritic cells isolated from wild-type C57BL/6 (+/+) mice, while human *OX40L* mRNA was detected in homozygous B-hOX40/hOX40L (H/H) mice.

OX40 protein expression analysis in splenocytes

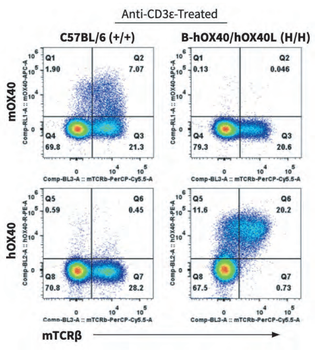

Species-specific OX40 protein expression analysis in wild-type and humanized B-hOX40/hOX40L mice. Following anti-CD3ε stimulation in vivo, splenocytes were isolated from wild-type C57BL/6 (+/+) and homozygous B-hOX40/hOX40L (H/H) mice and analyzed by flow cytometry using species-specific anti-OX40 antibodies. Murine OX40 protein was detected in wild-type mice, while human OX40 protein was detected in B-hOX40/hOX40L mice.

OX40L protein expression analysis in bone marrow-derived cells

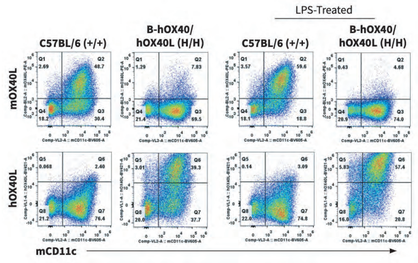

Species-specific OX40L protein expression analysis in wild-type and humanized B-hOX40/hOX40L mice. (Left) Bone marrow-derived cells were isolated from wild-type C57BL/6 (+/+) and homozygous B-hOX40/hOX40L (H/H) mice and analyzed by flow cytometry using species-specific anti-OX40L antibodies. (Right) Bone marrow-derived dendritic cells were stimulated with LPS and analyzed by flow cytometry using species-specific anti-OX40L antibodies. Murine OX40L protein was detected in wild-type mice, while human OX40L protein was detected in B-hOX40/hOX40L mice.

Spleen immune cell analysis in humanized B-hOX40/hOX40L mice

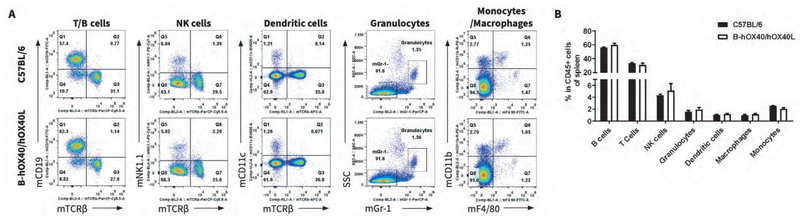

Analysis of spleen leukocytes in wild-type and humanized B-hOX40/hOX40L mice. Splenocytes were isolated from wild-type C57BL/6 and B-hOX40/hOX40L mice (female, n=3, 6-week-old) and analyzed by flow cytometry to assess leukocyte subpopulations. (A) Representative flow cytometry plots. Single live cells were gated on CD45+ and used for further analysis as indicated. (B) Percent of T cells, B cells, NK cells, dendritic cells, granulocytes, monocytes and macrophages in homozygous B-hOX40/hOX40L mice were similar to those in wild-type mice, demonstrating that OX40 and OX40L humanization does not change the overall development, differentiation or distribution of these spleen cells. Values are expressed as mean ± SEM.

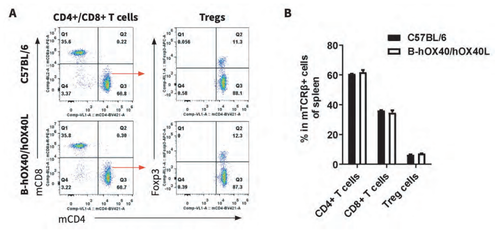

Analysis of spleen T cell subtypes in wild-type and humanized B-hOX40/hOX40L mice. Splenocytes were isolated from wild-type C57BL/6 and B-hOX40/hOX40L mice (female, n=3, 6-week-old) and analyzed by flow cytometry to assess T cell subtypes. (A) Representative flow cytometry plots. Single live CD45+ cells were gated on TCRβ+ and used for further analysis as indicated. (B) Percent of CD8+ T cells, CD4+ T cells, and Tregs in homozygous B-hOX40/hOX40L mice were similar to those in wild-type mice, demonstrating that OX40 and OX40L humanization does not change the overall development, differentiation or distribution of these spleen T cells. Values are expressed as mean ± SEM.

Blood immune cell analysis in humanized B-hOX40/hOX40L mice

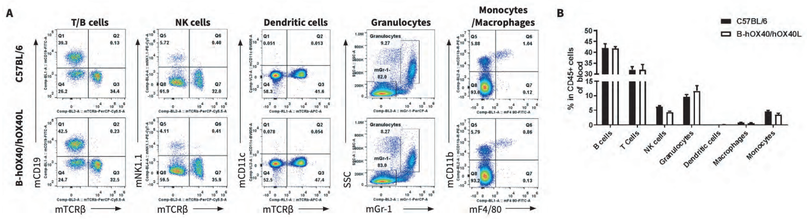

Analysis of blood leukocytes in wild-type and humanized B-hOX40/hOX40L mice. Blood cells were isolated from wild-type C57BL/6 and B-hOX40/hOX40L mice (female, n=5, 6-week-old) and analyzed by flow cytometry to assess leukocyte subpopulations. (A) Representative flow cytometry plots. Single live cells were gated on CD45+ and used for further analysis as indicated. (B) Percent of T cells, B cells, NK cells, dendritic cells, granulocytes, monocytes and macrophages in homozygous B-hOX40/hOX40L mice were similar to those in wild-type mice, demonstrating that OX40 and OX40L humanization does not change the overall development, differentiation or distribution of these blood cells. Values are expressed as mean ± SEM.

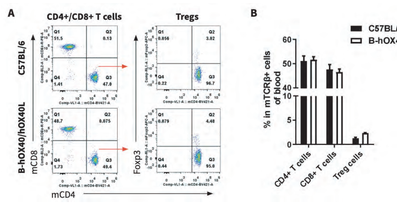

Analysis of blood T cell subtypes in wild-type and humanized B-hOX40/hOX40L mice. Blood cells were isolated from wild-type C57BL/6 and B-hOX40/hOX40L mice (female, n=3, 6-week-old) and analyzed by flow cytometry to assess T cell subtypes. (A) Representative flow cytometry plots. Single live CD45+ cells were gated on TCRβ+ and used for further analysis as indicated. (B) Percent of CD8+ T cells, CD4+ T cells, and Tregs in homozygous B-hOX40/hOX40L mice were similar to those in wild-type mice, demonstrating that OX40 and OX40L humanization does not change the overall development, differentiation or distribution of these blood T cell subtypes. Values are expressed as mean ± SEM.

Lymph node immune cell analysis in humanized B-hOX40/hOX40L mice

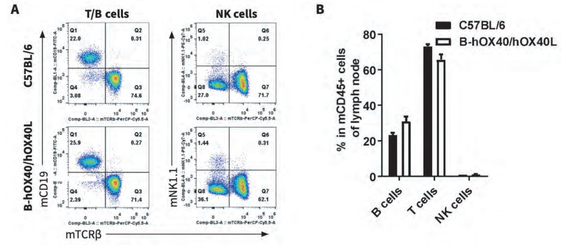

Analysis of lymph node leukocytes in wild-type and humanized B-hOX40/hOX40L mice. Lymph nodes were isolated from wild-type C57BL/6 and B-hOX40/hOX40L mice (female, n=3, 6-week-old) and analyzed by flow cytometry to assess leukocyte subpopulations. (A) Representative flow cytometry plots. Single live cells were gated on CD45+ and used for further analysis as indicated. (B) Percent of T cells, B cells, NK cells in homozygous B-hOX40/hOX40L mice were similar to those in wild-type mice, demonstrating that OX40 and OX40L humanization does not change the overall development, differentiation or distribution of these lymph node cells. Values are expressed as mean ± SEM.

Analysis of lymph node T cell subtypes in wild-type and humanized B-hOX40/hOX40L mice. Lymph nodes were isolated from wild-type C57BL/6 and B-hOX40/hOX40L mice (female, n=3, 6-week-old) and analyzed by flow cytometry to assess leukocyte subpopulations. (A) Representative flow cytometry plots. Single live CD45+ cells were gated on TCRβ+ and used for further analysis as indicated. (B) Percent of CD8+ T cells, CD4+ T cells, and Tregs in homozygous B-hOX40/hOX40L mice were similar to those in wild-type mice, demonstrating that OX40 and OX40L humanization does not change the overall development, differentiation or distribution of these lymph node T cells. Values are expressed as mean ± SEM.

CONCLUSIONS

mRNA expression analysis:
Mouse *Ox40l* mRNA was detected in dendritic cells isolated from wild-type mice, while human *OX40L* mRNA was detected in homozygous B-hOX40/hOX40L mice by RT-PCR.

Protein expression analysis:
Human OX40 and OX40L protein expression was detected in B-hOX40/hOX40L mice by flow cytometry.

Immune cell analysis:
OX40 and OX40L humanization does not change the overall development, differentiation or distribution of spleen, lymph node, and blood immune cells in B-hOX40/hOX40L mice.

biocytogen.com | info@biocytogen.com

5209

Generation of Humanized TREM2 Mice for Preclinical Evaluation of Therapeutics Targeting Tumor-Associated Macrophages

BIOCYTOGEN

BIOMICE

Ruili Lv[1], Jia Yu[1], Zhiyuan Shen[1], James Jin[2]

[1] Biocytogen (Pharmaceuticals) Beijing Co., Beijing, China; [2] Biocytogen Boston Corporation, Wakefield, MA, USA

ABSTRACT

In recent years, immune checkpoint inhibitors (ICIs) have improved treatment for several types of cancer. However, the overall response rates remain low, and drug resistance can occur in patients after initial responses. This resistance is thought to be due in part to tumor-associated macrophages (TAMs), which can deploy a number of mechanisms to suppress anti-tumor immunity, resulting in tumor immune escape.

Triggering receptor expressed on myeloid cells-2 (TREM2), a transmembrane receptor that is part of the immunoglobulin superfamily, is highly expressed on the surface of TAMs. Moreover, the expression level of TREM2 is reported to be higher in cancerous tissues vs normal tissues, with higher expression associated with poorer patient outcomes across multiple solid tumor types. Conversely, mice that lack *Trem2* experience slower tumor cell expansion and are more responsive to anti-PD-1 immunotherapy, suggesting that TREM2 may be a promising therapeutic target for improving responses to ICI immunotherapies.

To better assist the efficacy evaluation of anti-TREM2 antibodies, Biocytogen has generated a humanized TREM2 mouse model. In these mice, exons 1-5 and the 3'UTR of mouse *Trem2* gene, which encodes the full-length protein, were replaced by its human counterpart. In homozygous mice, human TREM2 protein expression is detected. The distribution of basal leukocyte subpopulations of blood, spleen, and lymph nodes in humanized B-hTREM2 mice were similar and comparable to those in wild-type C57BL/6 mice. Using the MC38 tumor model, we showed modest efficacy of an anti-human TREM2 antibody in inhibiting tumor growth in vivo. In summary, TREM2 humanized mice provide a powerful preclinical model for in vivo evaluation of anti-human TREM2 antibodies for cancer treatment.

Human *TREM2* Gene Expression Analysis

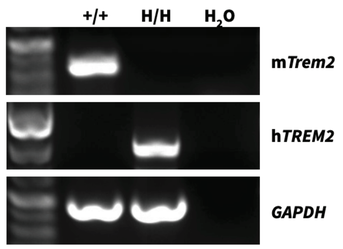

Species-specific *TREM2* gene expression analysis in wild-type and humanized B-hTREM2 mice by RT-PCR. Murine *Trem2* mRNA was detected in wild-type C57BL/6(+/+) mice, while human *TREM2* mRNA was detected in homozygous B-hTREM2(H/H) mice.

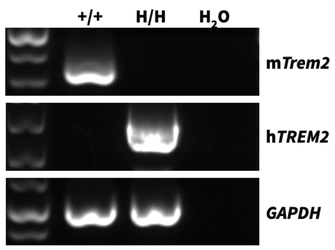

Species-specific *TREM2* gene expression analysis in wild-type and humanized B-hTREM2 mice(C) by RT-PCR. Murine *Trem2* mRNA was detected in wild-type BALB/c(+/+) mice(C), while human *TREM2* mRNA was detected in homozygous B-hTREM2(H/H) mice(C).

TREM2 Protein Expression Analysis

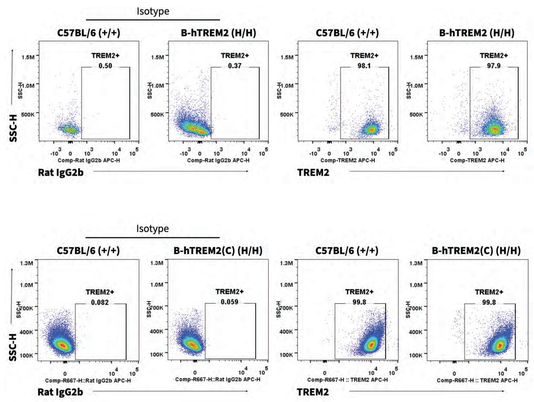

TREM2 protein expression analysis in wild-type and humanized B-hTREM2 mice. Microglia was isolated from wild-type C57BL/6(+/+) and homozygous B-hTREM2(H/H) mice and analyzed by flow cytometry using an anti- TREM2 antibody. Due to the cross- reactive antibody, TREM2 protein was detected in wild-type and B-hTREM2 mice.

TREM2 protein expression analysis in wild-type and humanized B-hTREM2 mice(C). Microglia was isolated from wild-type BALB/c(+/+) and homozygous B-hTREM2(H/H) mice(C) and analyzed by flow cytometry using an anti-TREM2 antibody. Due to the cross-reactive antibody, TREM2 protein was detected in wild-type and B-hTREM2 mice(C).

TREM2 Protein Expression Analysis in Tumor Cells Harvested From B-hTREM2 Mice

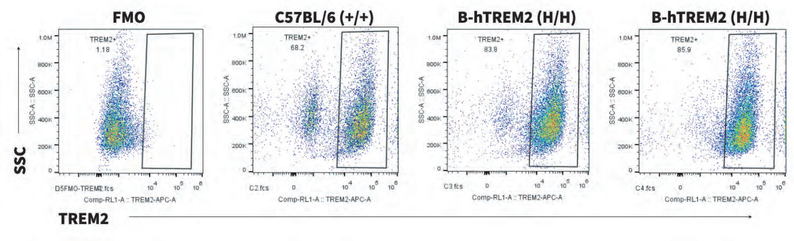

TREM2 protein expression analysis in tumor cells derived from wild-type and humanized B-hTREM2 mice. Murine colon cancer MC38 cells were inoculated into wild-type C57BL/6 (+/+) and homozygous B-hTREM2 (H/H) mice. Tumor tissues were harvested when tumor volume reached approximately 1000 mm^3 and analyzed by flow cytometry using an anti-TREM2 antibody. Due to the cross-reactive TREM2 antibody, TREM2 protein was detected in tumor macrophages from wild-type and homozygous B-hTREM2 mice.

Human TREM2 Protein Expression Analysis in B-hTREM2 Mice

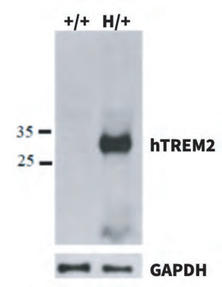

Human TREM2 protein expression analysis in wild-type and humanized B-hTREM2 mice. Brain tissue was isolated from wild-type C57BL/6 (+/+) and heterozygous B-hTREM2 (H/+) mice and analyzed by western blot using an anti-human TREM2 antibody. Human TREM2 protein was not detected in wild-type mice but was detected in B-hTREM2 mice.

In vivo Efficacy Evaluation Using an Anti-Human TREM2 Antibody

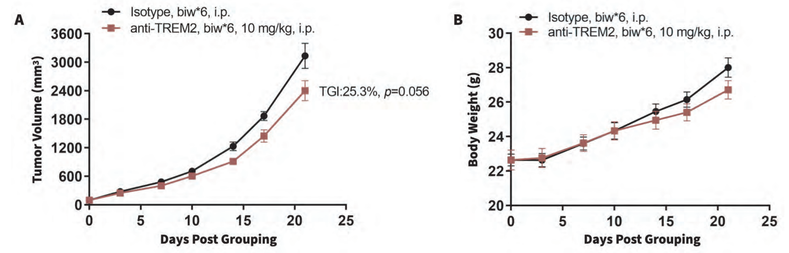

Anti-tumor activity of an anti-human TREM2 antibody in humanized B-hTREM2 mice. Murine colon cancer MC38 cells were subcutaneously implanted into homozygous B-hTREM2 mice (male, 6-7-week-old, n=6). Mice were grouped and treated with an anti-human TREM2 antibody (analog) at the dose and schedule as indicated when the tumor volume reached approximately 100 mm^3. (A) The anti-human TREM2 antibody controlled MC38 tumor growth in B-hTREM2 mice, (B) without negatively impacting body weight changes. This demonstrates that B-hTREM2 mice are a powerful preclinical model for *in vivo* evaluation of anti-human TREM2 antibodies. Values are expressed as mean ± SEM.

In vivo Efficacy Evaluation of an Anti-Human TREM2 Antibody in B-hTREM2 Mice(C)

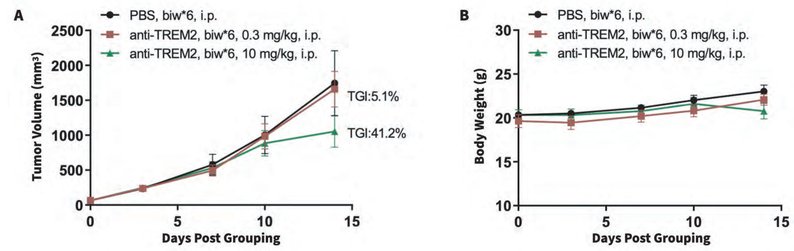

Anti-tumor activity of an anti-human TREM2 antibody in humanized B-hTREM2 mice(C). Murine breast carcinoma EMT-6 cells were subcutaneously implanted into homozygous B-hTREM2 mice(C) (female, 10-week-old, n=6). Mice were grouped and treated with an anti-human TREM2 antibody (analog) at the dose and schedule as indicated when the tumor volume reached approximately 50-80 mm^3. (A) High dose of the anti-human TREM2 antibody controlled EMT-6 tumor growth in B-hTREM2 mice(C), (B) without negatively impacting body weight changes. This demonstrates that B-hTREM2 mice(C) are a powerful preclinical model for *in vivo* evaluation of anti-human TREM2 antibodies. Values are expressed as mean ± SEM.

CONCLUSIONS

- Murine *Trem2* mRNA was detected in wild-type mice, while human *TREM2* mRNA was detected in homozygous B-hTREM2 mice by RT-PCR.
- TREM2 protein was detected in microglia and tumor-derived macrophages isolated from wild-type and homozygous B-hTREM2 mice by flow cytometry.
- Human TREM2 protein was detected in B-hTREM2 mice by western blot using an anti-human TREM2 antibody.
- Anti-human TREM2 antibody (analog) was effective in controlling MC38 and EMT-6 tumor growth in B-hTREM2 mice.

biocytogen.com | info@biocytogen.com

4592

In vivo Efficacy Evaluation of Anti-Human VEGFR2 Antibodies in Humanized B-hVEGFR2 Mice

BIOCYTOGEN

BIOMICE

Lei Zhao[1], Chengzhang Shang[1], Rebecca Soto[2], Chonghui Liu[1], Zhaoxue Yu[2]

[1] Biocytogen (Pharmaceuticals) Beijing Co., Beijing, China; [2] Biocytogen Boston Corporation, Wakefield, MA, USA

ABSTRACT

Angiogenesis, vascular development, vascular permeability, and embryonic hematopoiesis is partly regulated by VEGF binding to VEGFR2, which forms receptor dimers and activates downstream signaling pathways. In addition to developmental cues, VEGFR2 is also associated with disease progression for psoriasis, rheumatoid arthritis, diabetic retinopathy, and more significantly, tumor growth and drug resistance. Given this, inhibition of VEGFR2 signaling is actively being studied, and multiple VEGFR2 inhibitors have entered various phases of clinical studies and have shown promising results. To evaluate in vivo efficacy of anti-human VEGFR2 antibodies, we generated a human VEGFR2 knock-in (B-hVEGFR2) mouse model by replacing the murine *Vegfr2* extracellular domain sequence with the corresponding human sequence. We validated human VEGFR2 gene and protein expression in B-hVEGFR2 mice by RT-PCR and flow cytometry, respectively. Furthermore, we observed an anti-tumor effect with anti-human VEGFR2 antibodies in homozygous B-hVEGFR2 mice subcutaneously implanted with MC38 colon cancer cells. Taken together, we established a novel preclinical B-hVEGFR2 mouse model for evaluation of VEGFR2-targeted immunotherapy.

VEGFR2 Gene Expression Analysis in B-hVEGFR2 Mice

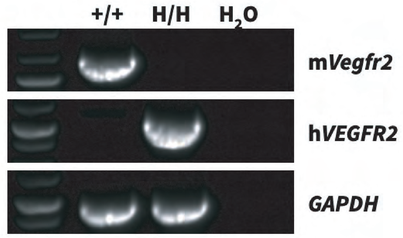

Species-specific *VEGFR2* gene expression analysis in wild-type and humanized B-hVEGFR2 mice by RT-PCR. Murine *Vegfr2* mRNA was detected in embryonic tissue isolated from wild-type C57BL/6 (+/+) mice, while human *VEGFR2* mRNA was detected in homozygous B-hVEGFR2 (H/H) mice.

VEGFR2 Protein Expression Analysis in B-hVEGFR2 Mice

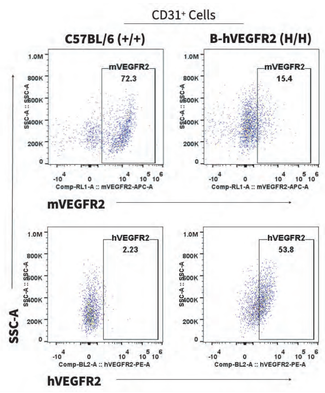

Species-specific VEGFR2 protein expression analysis in wild-type and humanized B-hVEGFR2 mice. Embryonic lung endothelial cells were isolated from wild-type C57BL/6 (+/+) and homozygous B-hVEGFR2 (H/H) mice and analyzed by flow cytometry using species-specific anti-VEGFR2 antibodies. Anti-mouse VEGFR2 antibody was cross-reactive between mouse and human. Combined with mRNA expression in wild-type and homozygous B-hVEGFR2 mice, it can be proved that mouse VEGFR2 was detectable in wild-type mice. Human VEGFR2 was exclusively detectable in homozygous B-hVEGFR2 mice (H/H) but not in wild-type mice

Immune Cell Analysis in B-hVEGFR2 Mice

Spleen immune cell analysis in wild-type and humanized B-VEGFR2 mice. Splenocytes were isolated from wild-type C57BL/6 and B-hVEGFR2 mice (female, n=3, 6-week-old) and analyzed by flow cytometry to assess leukocytes.
(A) Representative flow cytometry plots. Single live cells were gated on CD45+ cells and used for further analysis as indicated. (B) Percent of T cells, B cells, NK cells, dendritic cells, granulocytes, monocytes and macrophages in homozygous B-hVEGFR2 mice were similar to those in wild-type mice, demonstrating that VEGFR2 humanization does not change the overall development, differentiation or distribution of these splenic cell types. Values are expressed as mean ± SEM.

Immune Cell Analysis in B-hVEGFR2 Mice (continued)

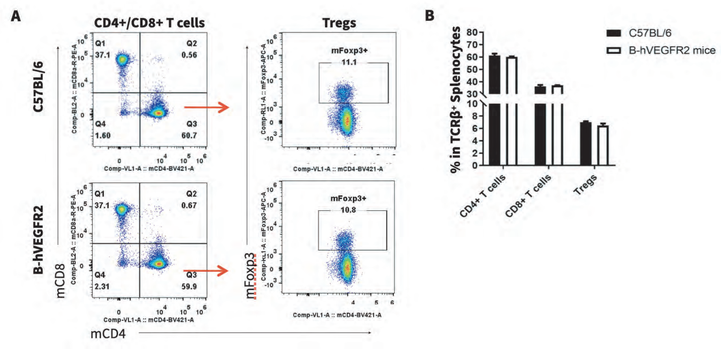

Spleen immune cell analysis in wild-type and humanized B-VEGFR2 mice. Splenocytes were isolated from wild-type C57BL/6 and B-hVEGFR2 mice (female, n=3, 6-week-old) and analyzed by flow cytometry to assess leukocytes. (A) Representative flow cytometry plots. Single live CD45+ cells were gated on TCRβ+ T cells and used for further analysis as indicated. (B) Percent of CD4+ T cells, CD8+ T cells, and Tregs in homozygous B-hVEGFR2 mice were similar to those in wild-type mice, demonstrating that VEGFR2 humanization does not change the overall development, differentiation or distribution of these splenic T cell subtypes. Values are expressed as mean ± SEM.

In vivo Efficacy Evaluation of an Anti-Human VEGFR2 Antibody

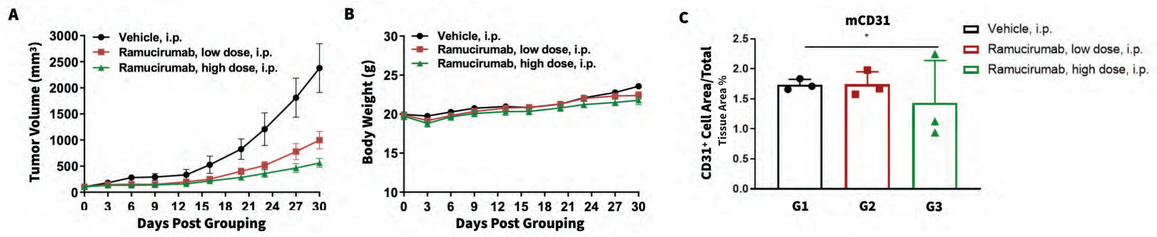

Antitumor activity of anti-human VEGFR2 antibody in B-hVEGFR2 mice. Murine colon cancer MC38 cells were subcutaneously implanted into homozygous B-hVEGFR2 mice (female, 8-week-old, n=6). Mice were grouped when tumor volume reached approximately 100 mm^3, at which time they were treated with different doses of an anti-human VEGFR2 antibody (Ramucirumab, in house). (A) Ramucirumab inhibited MC38 tumor growth in B-hVEGFR2 mice, (B) without negatively impacting body weight. (C) Ramucirumab inhibits vascular endothelial cell proliferation. Values are expressed as mean ± SEM.

CONCLUSIONS

mRNA expression analysis:
Murine *Vegfr2* mRNA was detected in embryonic tissue isolated from wild-type mice, while human *VEGFR2* mRNA was detected in B-hVEGFR2 mice.

Protein expression analysis:
Murine VEGFR2 protein was detected in wild-type mice, while human VEGFR2 protein was detected in B-hVEGFR2 mice.

In vivo efficacy:
Anti-human VEGFR2 antibody was effective in controlling MC38 tumor growth in B-hVEGFR2 mice and inhibits vascular endothelial cell proliferation.

biocytogen.com | info@biocytogen.com

5208

Development of Immunodeficient Mice Expressing Human IL3, GM-CSF, CSF1 and THPO for Improved Human Myeloid and Lymphoid Cell Reconstitution

BIOCYTOGEN

BIOMICE

Ruili Lv[1], Yanhui Nie[1], Jing Zhang[1], Jenna Frame[2], Qiang Liu[1], James Jin[2]

[1] Biocytogen (Pharmaceuticals) Beijing Co., Beijing, China; [2] Biocytogen Boston Corporation, Wakefield, MA, USA

biocytogen.com | info@biocytogen.com

ABSTRACT

Mice reconstituted with human immune cells are essential tools to study human immune reactions in vivo, including those involving cancer immunotherapies. A major limitation of these models is the poor development of human myeloid cells to mediate effective human immune cell-tumor interactions. This is because hematopoietic cells are highly dependent on several human cytokines for efficient differentiation, maturation, and survival. THPO (thrombopoietin) can enhance the maintenance of functional human hematopoietic stem cells, and stimulates the production and differentiation of megakaryocytes, which produce large numbers of platelets in the bone marrow. IL3 (interleukin 3), GM-CSF (granulocyte-macrophage colony-stimulating factor, CSF2) and CSF1 (macrophage colony-stimulating factor, M-CSF) are cytokines that promote the proliferation and differentiation of a variety of myeloid cells, including monocytes, macrophages, granulocytes, dendritic cells, and platelets. Because these cytokines lack sufficient cross-reactivity between human and mice, it is difficult to reconstitute human immune cells of these lineages in immunodeficient mice. Therefore, we predict that genetic humanization of these four cytokines will improve the reconstitution of human myeloid cells in immunodeficient mice. We engineered an M-CSF, GM-CSF, THPO, and IL3 humanized strain in the background of B-NDG mice (NOD.CB17-*Prkdc*^{scid} *Il2rg*^{tm1} /Bcgen), termed B-NDG MGMT3 mice. The full sequences of mouse *Il3, Csf2, Csf1* and *Thpo* genes (except the UTRs) were respectively replaced with the coding sequences (CDS) of human *IL3, CSF2, CSF1* and *THPO* genes. Human GM-CSF, CSF1 and THPO proteins were confirmed to be expressed by ELISA in B-NDG MGMT3 mice. Human CD34$^+$ HSCs (3E4) were intravenously engrafted into wild-type B-NDG mice and homozygous B-NDG MGMT3 male and female newborn mice via the temporal vein. B-NDG mice were treated with 1.0 Ggamma irradiation, while B-NDG MGMT3 mice were not irradiated. The survival rate of B-NDG MGMT3 mice was similar to B-NDG mice until 16 weeks post-CD34$^+$ engraftment. However, the body weight of B-NDG MGMT3 mice was significantly higher than that of B-NDG mice. Analysis of peripheral blood lymphocytes showed that the proportion of hCD45$^+$ cells in B-NDG MGMT3 mice reached 25% starting from 12 weeks after engraftment and continued to rise; levels were significantly higher than that observed in B-NDG mice. The proportions and cell number of T cells, NK cells, monocytes, MDSCs, DCs and Tregs engrafted in B-NDG MGMT3 mice were higher than B-NDG mice. The results indicate that B-NDG MGMT3 mice are a novel humanized model for human myeloid and lymphocytic cell reconstitution that does not require preconditioning.

GM-CSF, CSF1 and THPO Protein Expression Analysis in B-NDG and B-NDG MGMT3 Immunodeficient Mice

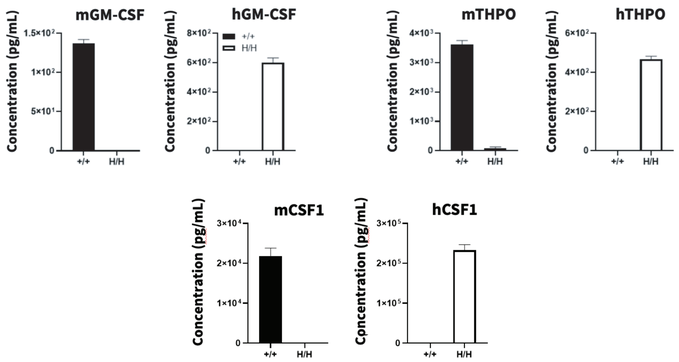

Species-specific GM-CSF, CSF1 and THPO protein expression analysis in B-NDG and B-NDG MGMT3 mice. Serum was collected from wild-type B-NDG$^{(+/+)}$ and homozygous B-NDG MGMT3$^{(H/H)}$ mice stimulated with LPS in vivo and analyzed by ELISA (n=3). Mouse GM-CSF, CSF1 and THPO proteins were detected in B-NDG mice, while human GM-CSF, CSF1 and THPO proteins were detected in B-NDG MGMT3 mice. B-NDG mice lack mature T cells, therefore IL3 was not detected.

Survival Rate of B-NDG and B-NDG MGMT3 Immunodeficient Mice After CD34$^+$ HSC Engraftment

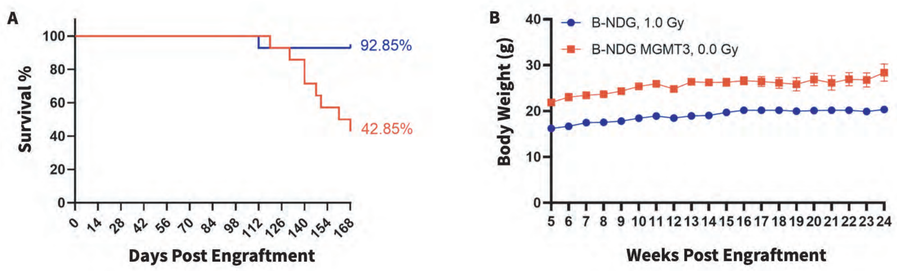

Human immune system reconstitution in B-NDG and B-NDG MGMT3 mice. Wild-type B-NDG and homozygous B-NDG MGMT3 mice were engrafted with human CD34$^+$ HSCs (3E4) by intravenous injection (temporal vein) (both sex, 24-72 hr after birth, n=15). B-NDG mice were treated with 1.0 Gy-irradiation, B-NDG MGMT3 mice were not irradiated. (A) Survival rates were analyzed by Kaplan Meier survival curves. Results showed that the survival rate of B-NDG MGMT3 mice was similar to B-NDG mice until 18 weeks after human CD34$^+$ HSC engraftment and then decreased to 42.85% at 24 weeks post engraftment. (B) Body weight changes of B-NDG MGMT3 mice were higher than that of B-NDG mice. Values are expressed as mean ± SEM. HSCs: hematopoietic stem cells.

Proportion of Human Immune Cell Populations Reconstituted in B-NDG and B-NDG MGMT3 Mice

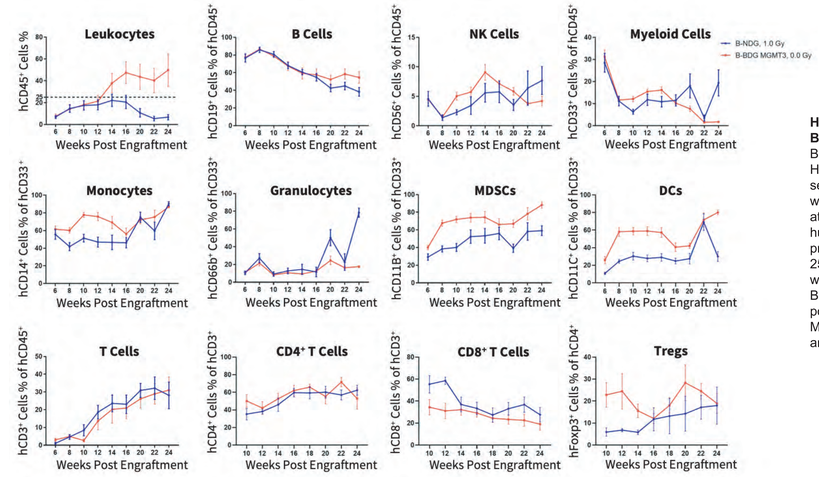

Human immune system reconstitution in B-NDG and B-NDG MGMT3 mice. Wild-type B-NDG and homozygous B-NDG MGMT3 mice were engrafted with human CD34$^+$ HSCs (3E4) by intravenous injection (temporal vein) (both sex, 24-72 hr after birth, n=15). B-NDG mice were treated with 1.0 Gy-irradiation, B-NDG MGMT3 mice were not irradiated. Peripheral blood reconstitution after engraftment with human CD34$^+$ HSCs was analyzed by flow cytometry. The proportion of hCD45$^+$ cells in B-NDG MGMT3 mice reached 25% after 12 weeks post-engraftment and continued to rise, while the proportion of hCD45$^+$ cells remained steady in B-NDG mice and began to decline after 16 weeks. The proportion of monocytes, MDSCs, DCs and Tregs in B-NDG MGMT3 mice were higher than that in B-NDG mice. Values are expressed as mean ± SEM.

Leukocyte and Lymphocyte Cell Numbers Reconstituted in B-NDG and B-NDG MGMT3 Mice

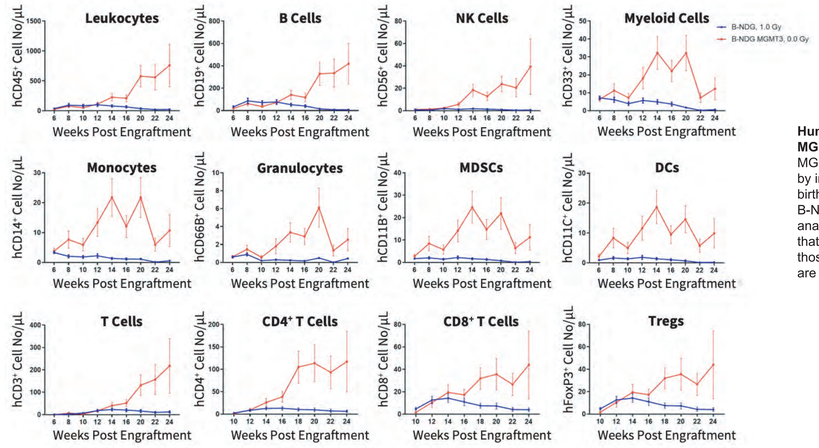

Human immune system reconstitution in B-NDG and B-NDG MGMT3 mice. Wild-type B-NDG and homozygous B-NDG MGMT3 mice were engrafted with human CD34$^+$ HSCs (3E4) by intravenous injection (temporal vein) (both sex, 24-72 hr after birth, n=15). B-NDG mice were treated with 1.0 Gy-irradiation, B-NDG MGMT3 mice were not irradiated. Flow cytometric analysis of peripheral blood leukocytes and lymphocytes showed that human cell numbers in B-NDG MGMT3 mice surpassed those in B-NDG mice after 12 weeks post-engraftment. Values are expressed as mean ± SEM.

CONCLUSIONS

- We generated an immunodeficient (B-NDG) mouse model containing human GM-CSF, CSF1, THPO, and IL3 in place of the murine counterparts. Human GM-CSF, CSF1 and THPO proteins were detected in B-NDG MGMT3 mice. As B-NDG mice lack mature T cells, IL3 was not detected.
- The survival rate of B-NDG MGMT3 mice after human CD34+ HSC engraftment was similar to that of B-NDG mice until 18 weeks post-engraftment.
- The proportion of CD45+ cells in B-NDG MGMT3 mice reached 25% after 12 weeks post-engraftment and continued to rise higher than levels observed in B-NDG mice. The proportion and number of monocytes, MDSCs, DCs and Tregs in B-NDG MGMT3 mice were also higher in B-NDG MGMT3 mice compared to B-NDG mice.
- B-NDG MGMT3 mice are a novel humanized model for human myeloid and lymphocytic cell reconstitution that does not require preconditioning.

5207

Development of MHC I/II Knock-out Immunodeficient Mouse Strains for Alleviating GvHD Induced by Human PBMC Reconstitution

Qiang Liu[1], Chengzhang Shang[1], Xiaofei Zhou[1], Jenna Frame[2], Zhiyuan Shen[1], Zhaoxue Yu[2]

[1] Biocytogen (Pharmaceuticals) Beijing Co., Beijing, China; [2] Biocytogen Boston Corporation, Wakefield, MA, USA

biocytogen.com | info@biocytogen.com

ABSTRACT

Severely immunodeficient mouse strains, such as B-NDG mice, lack B, T, and NK cells, and have been widely used as an in vivo model to evaluate human immune responses, including applications in immuno-oncology in recent years. However, when human peripheral blood mononuclear cells (PBMCs) are engrafted in these mice, severe acute xenogeneic graft-versus-host disease (GvHD) arises due to engagement of human T cell receptors (TCRs) with major histocompatibility complex (MHC) proteins I and II on the surface of murine immune cells. GvHD shortens the animal life span such that there is only a brief window of evaluation of human immune cell functions in these mouse models. Consequently, efforts have been undertaken to reduce human PBMC-induced GvHD and to subsequently extend the window of human immunity assessment in immunodeficient mouse strains by eliminating mouse MHC I and MHC II. We previously engineered a novel B2m gene knock-out strain on the B-NDG background (NOD.CB17-*Prkdc*^{scid} *Il2rg*^{tm1} /Bcgen), which is deficient in MHC I expression, but expresses the B2m gene fused into the FcRn gene to retain FcRn-mediated antibody metabolism. In order to eliminate MHC II expression, we also engineered an H2-Ab1 gene knock-out strain on the same B-NDG background and cross-bred the two strains together to obtain an MHC I/II double KO mouse model, termed B-NDG MHC I/II DKO mice plus. Splenocytes collected from the engineered strains were analyzed by flow cytometry. As expected, mouse H-2K^b/H-2D^b was not detectable in B-NDG B2m KO plus mice or B-NDG MHC I/II DKO mice plus. While mouse I-A^k was detected in B-NDG mice and B-NDG B2m KO plus mice, it was not detected in B-NDG MHC I/II DKO mice plus. Pharmacokinetic assessments demonstrate that B-NDG mice and B-NDG B2m KO mice plus groups were able to recycle human IgG, with no differences when compared with wild-type C57BL/6 mice, indicating normal FcRn function. Finally, the three strains of mice were irradiated and engrafted with human PBMC from three donors to evaluate GvHD incidence. As expected, the reconstitution levels of CD45+ leukocytes, T cells, CD4+ T cells, CD8+ T cells, Tregs and NK cells were similar among the three strains. However, lack of MHC I/II in B-NDG MHC I/II DKO mice plus can significantly extend the life span and reduce GvHD induced by human PBMC engraftment compared to B-NDG mice and B-NDG B2m KO mice plus. These results indicate that B-NDG MHC I/II DKO mice plus provides a useful mouse model for reducing GvHD after human PBMC reconstitution in immunodeficient mice. This model may be a powerful preclinical tool for future in vivo evaluation of cell therapies and antibodies.

Generation of Immunodeficient Mice that Lack MHC-I and MHC-II

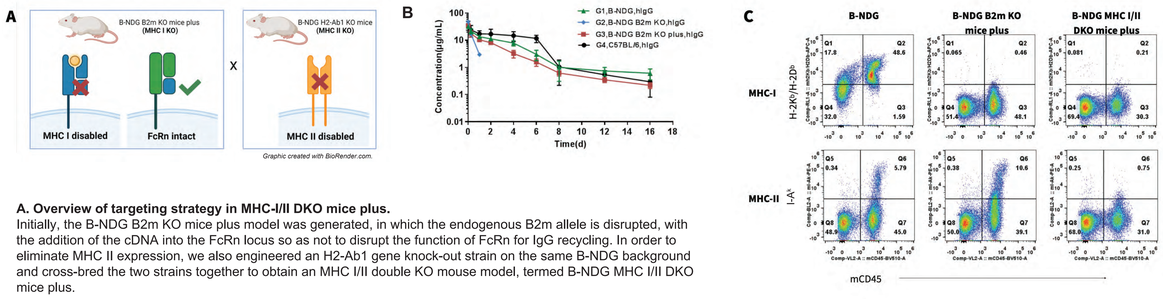

A. Overview of targeting strategy in MHC-I/II DKO mice plus.
Initially, the B-NDG B2m KO mice plus model was generated, in which the endogenous B2m allele is disrupted, with the addition of the cDNA into the FcRn locus so as not to disrupt the function of FcRn for IgG recycling. In order to eliminate MHC II expression, we also engineered an H2-Ab1 gene knock-out strain on the same B-NDG background and cross-bred the two strains together to obtain an MHC I/II double KO mouse model, termed B-NDG MHC I/II DKO mice plus.

B. Pharmacokinetic assessments of B-NDG B2m KO mice plus indicates normal IgG recycling.
Homozygous B-NDG, B-NDG B2m mice, B-NDG B2m KO mice plus and C57BL/6 mice were treated with human IgG (n=5). Blood samples were collected at different time points. Pharmacokinetic assessments indicate that B-NDG and B-NDG B2m KO mice plus groups were able to maintain human IgG at levels similar to WT mice. In contrast, the drug concentration of B-NDG B2m KO mice group was below detection after 2 days.

C. Strain-specific H-2K^b/H-2D^b (MHC-I) and I-A^k (MHC-II) protein expression analysis in B-NDG, B-NDG B2m KO plus and B-NDG MHC I/II DKO mice plus. Splenocytes were isolated from B-NDG, B-NDG B2m KO plus and B-NDG MHC I/II DKO mice plus and analyzed by flow cytometry to assess H-2K^b/H-2D^b and I-A^k expression. Mouse H-2K^b/H-2D^b was detected in B-NDG mice but not in B-NDG B2m KO plus mice or B-NDG MHC I/II DKO mice plus. Mouse I-A^k was detected in B-NDG mice and B-NDG B2m KO plus mice but not in B-NDG MHC I/II DKO mice plus.

Comparison of GvHD Severity in Immunodeficient Mice

Comparison of GvHD severity induced by human PBMC engraftment in B-NDG mice, B-NDG B2m KO mice plus and B-NDG MHC I/II DKO mice plus. Immunodeficient B-NDG mice, B-NDG B2m KO mice plus and B-NDG MHC I/II DKO mice plus (female, 5-weeks-old, n=5) were engrafted intravenously with human peripheral blood mononuclear cells (PBMCs, 5 × 10^6) from three healthy donors (Donor 1-3) on day 0. Survival rates of mice were analyzed by Kaplan Meier survival curves. Body weight changes were measured twice weekly. Clinical signs of GvHD were scored twice a week. Results were graphed (A) by donor and (B) by mouse strain. Together, the data indicates that MHC I/II double knock-out in B-NDG MHC I/II DKO mice plus can significantly extend the life span and reduce GvHD severity when compared to B-NDG mice and B-NDG B2m KO mice plus. Therefore, B-NDG MHC I/II DKO mice plus are a suitable mouse model for human PBMC engraftment. Values were expressed as mean ± SEM.

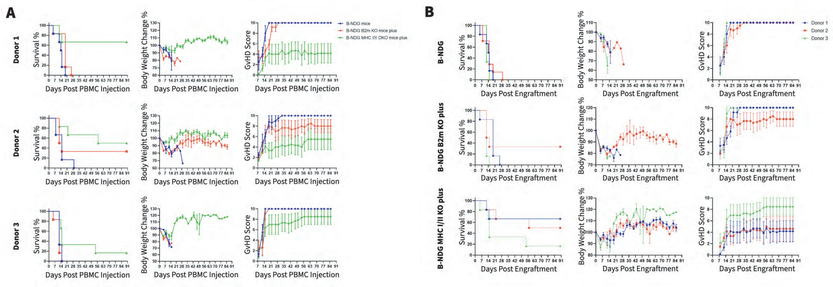

Human PBMC Reconstitution in B-NDG Mice, B-NDG B2m KO Mice Plus and B-NDG MHC I/II DKO Mice Plus

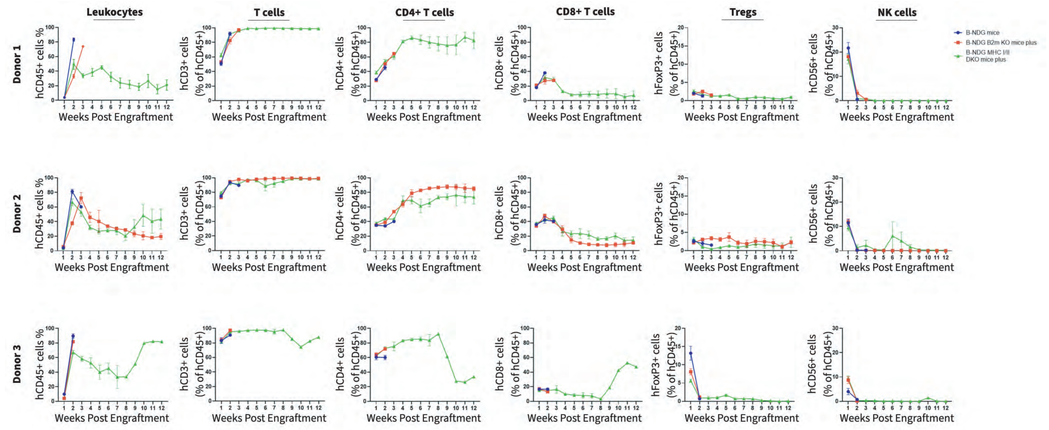

Comparison of reconstitution levels of human PBMCs in B-NDG mice, B-NDG B2m KO mice plus and B-NDG MHC I/II DKO mice plus. B-NDG mice, B-NDG B2m KO plus mice, and B-NDG MHC I/II DKO mice plus were intravenously injected with human PBMCs (5E6) derived from three healthy donors (donor1-3) on day 0 (n = 5, female, 5 weeks old). Peripheral blood was sampled weekly to analyze the reconstitution level of human immune cells. The experiment was ended 90 days after reconstitution. The results showed that 2 weeks after hPBMC reconstitution in B-NDG MHC I/II DKO mice plus, the proportion of reconstituted human CD45+ cells was more than 50%, but slightly lower than the levels in B-NDG mice and B-NDG B2m KO plus mice. The majority of human cells were human T cells. The proportion of the cells was similar among the three strains of mice. Donor 3-derived human PBMCs showed the highest reconstitution levels (human CD45+ cells, CD4+ T cells). The results indicated that human PBMCs from different donor sources had an effect on reconstitution, but the impact on B-NDG MHC I/II DKO mice plus reconstitution was not as pronounced as in B-NDG mice and B-NDG B2m KO plus mice. Reconstitution levels in B-NDG MHC I/II DKO mice plus, although slightly lower than the other two strains of mice, remained high. Regardless of the strain of mice engrafted, the higher the reconstitution level of human T cells, especially human CD4+ T cells, the more severe the GvHD. Thus, B-NDG MHC I/II DKO mice plus are a more suitable immunodeficient mouse model for reconstitution of the human immune system using human PBMCs.

Analysis of Peripheral Blood Leukocytes in B-NDG Mice, B-NDG B2m KO Mice Plus and B-NDG MHC I/II DKO Mice Plus

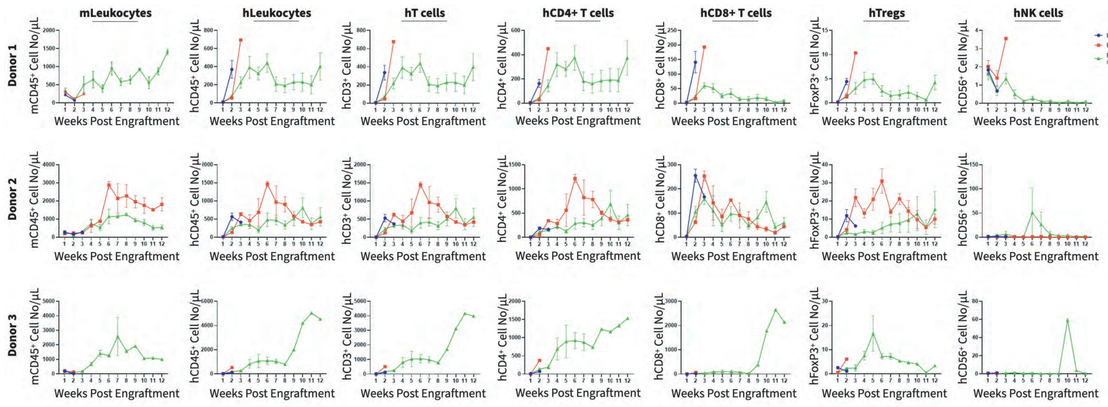

Comparison of reconstitution levels of human PBMCs in B-NDG mice, B-NDG B2m KO mice plus and B-NDG MHC I/II DKO mice plus. B-NDG mice, B-NDG B2m KO plus mice, and B-NDG MHC I/II DKO mice plus were intravenously injected with human PBMCs (5E6) derived from three healthy donors (donor1-3) on day 0 (n = 5, female, 5 weeks old). Peripheral blood was sampled weekly to analyze the reconstitution level of human immune cells. The experiment was ended 90 days after reconstitution. The results showed that regardless of which donor-derived PBMCs were implanted, various types of human T cells could be reconstituted in B-NDG MHC I/II DKO mice plus. However, the numbers of all reconstituted cells in B-NDG MHC I/II DKO mice plus were lower than those in B-NDG mice and B-NDG B2m KO plus mice. Donor 3 has the most severe GvHD; this donor reconstituted the largest number of human T cells and CD4+ T cells.

CONCLUSIONS

- We have generated an immunodeficient model, B-NDG MHC I/II DKO mice plus, that lacks both MHC-I and MHC-II.
- Protein expression analysis confirms that B-NDG MHC I/II DKO mice plus lack Mouse H-2K^b/H-2D^b and Mouse I-A^k.
- B-NDG MHC I/II DKO mice plus mice displayed an extended life span and reduced GvHD following human PBMC engraftment when compared to B-NDG mice and B-NDG B2m KO mice plus.
- B-NDG MHC I/II DKO mice plus is an ideal immunodeficient model for extended engraftment of human PBMCs.

3233

A Novel Triple Humanized B-hPD-1/hPD-L1/hCCR8 Mouse Model to Evaluate in vivo Efficacy of Combination Therapies

Linlin Wang[1], Xiao Liu[1], James Jin[2], Yuxiang Yu[1]

[1] Biocytogen (Pharmaceuticals) Beijing Co., Beijing, China; [2] Biocytogen Boston Corporation, Wakefield, MA, USA

ABSTRACT

Regulatory T cells (Tregs) play an immunosuppressive role in the tumor microenvironment (TME), such that altering or depleting Treg function has emerged as an important anti-tumor strategy. Targeting CCR8, which is highly expressed in tumor-infiltrating Tregs, has shown its potency in reducing tumor burden and increasing responsiveness to immune-checkpoint blockade therapy. Collectively, this suggests a need for pre-clinical models that support Treg-targeted therapies. To address this, Biocytogen developed a triple humanized (B-hPD-1/hPD-L1/hCCR8) mouse model to evaluate in vivo efficacy of combination therapies. In this model, the full coding sequence of murine *Ccr8* was replaced by the full coding sequence of human *CCR8*, while murine *Pd-1* and *Pd-l1* IgV domains were replaced by their human counterpart gene sequences. Human PD-1 and PD-L1 protein expression was confirmed in B-hPD-1/hPD-L1/hCCR8 mice by flow cytometry, and human CCR8 protein expression was observed in MC38 tumors harvested from B-hPD-1/hPD-L1/hCCR8 mice. Finally, combination therapy using anti-human PD-1 and anti-human CCR8 antibodies were effective in controlling B-hPD-L1 MC38 tumor growth in B-hPD-1/hPD-L1/hCCR8 mice. Altogether, this line provides a powerful preclinical model for in vivo evaluation of therapeutic antibodies. antibodies.

PD-1 Protein Expression Analysis in B-hPD-1/hPD-L1/hCCR8 mice

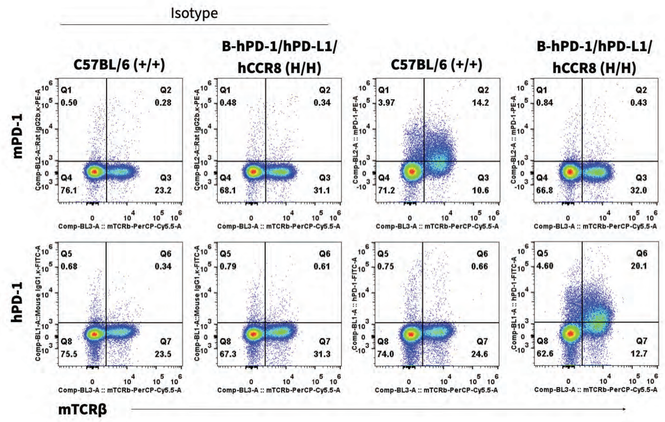

Species-specific PD-1 protein expression analysis in wild-type and humanized B-hPD-1/hPD-L1/hCCR8 mice. Following anti-CD3ε stimulation *in vivo* (7.5 μg/mice, 24 hours, i.p.), splenocytes were isolated from wild-type C57BL/6 (+/+) and homozygous B-hPD-1/hPD-L1/ hCCR8 (H/H) mice and analyzed by flow cytometry using species-specific anti-PD-1 antibodies. Mouse PD-1 protein was detected in wild-type mice, while human PD-1 protein was detected in B-hPD-1/hPD-L1/ hCCR8 mice.

PD-L1 Protein Expression Analysis in B-hPD-1/hPD-L1/hCCR8 Mice

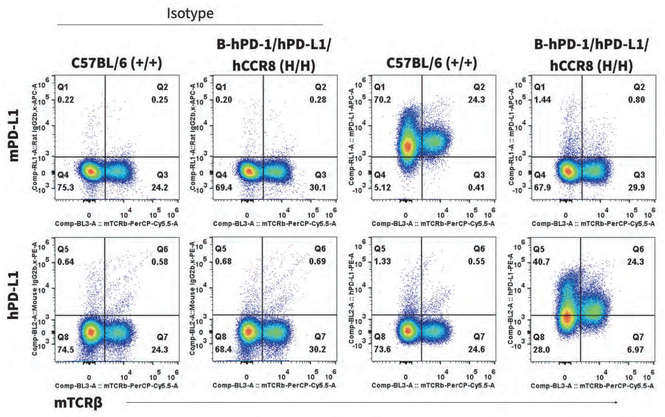

Species-specific PD-L1 protein expression analysis in wild-type and humanized B-hPD-1/hPD-L1/hCCR8 mice. Following anti-CD3ε stimulation *in vivo* (7.5 μg/mice, 24 hours, i.p.), splenocytes were isolated from wild-type C57BL/6 (+/+) and homozygous B-hPD-1/hPD-L1/ hCCR8 (H/H) mice and analyzed by flow cytometry using species-specific anti-PD-L1 antibodies. Mouse PD-L1 protein was detected in wild-type mice, while human PD-L1 protein was detected in B-hPD-1/hPD-L1/ hCCR8 mice.

CCR8 Protein Expression Analysis in B-hPD-1/hPD-L1/hCCR8 mice

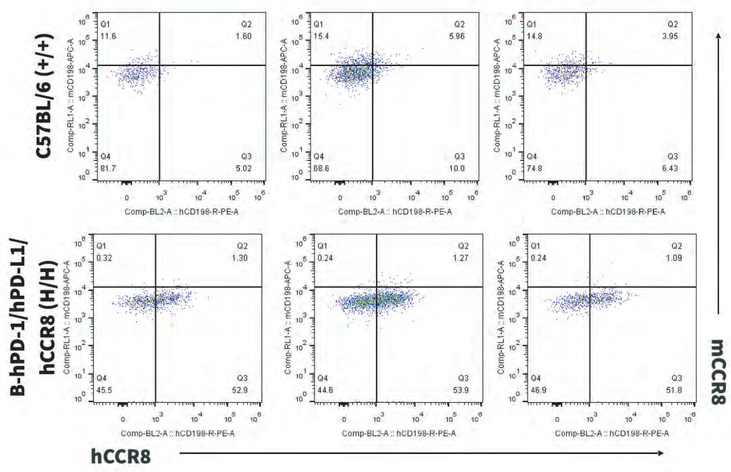

Species-specific CCR8 protein expression analysis in wild-type and humanized B-hPD-1/hPD-L1/hCCR8 mice. Murine colon cancer MC38 cells were inoculated into wild-type C57BL/6 (+/+) and homozygous B-hPD-1/hPD-L1/hCCR8 (H/H) mice. When the volume reached approximately 500mm^3, tumors were harvested and analyzed by flow cytometry using species-specific anti-CCR8 antibodies. Mouse CCR8 protein was detected on Tregs from wild-type mice, while human CCR8 protein was detected on Tregs from B-hPD-1/hPD-L1/hCCR8 mice.

Combination Therapy Using Anti-Human PD-1 and CCR8 Antibodies

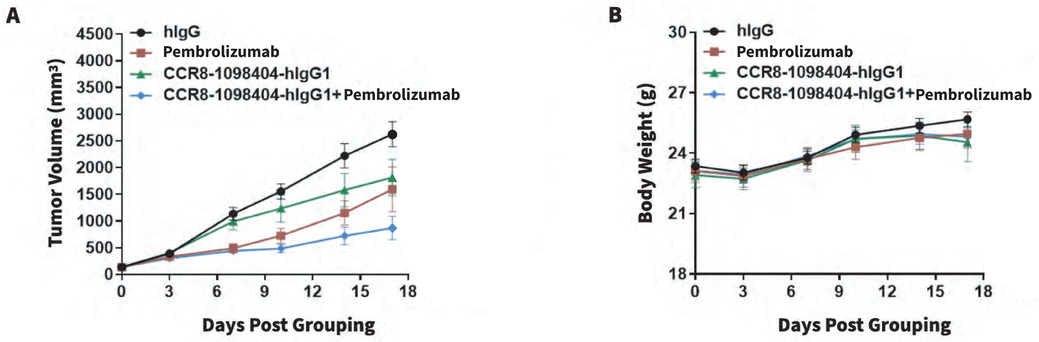

Antitumor activity of an anti-human PD-1 antibody combined with an anti-human CCR8 antibody in B-hPD-1/hPD-L1/hCCR8 mice. Humanized murine colon cancer B-hPD-L1 MC38 plus cells were subcutaneously implanted into homozygous B-hPD-1/hPD-L1/hCCR8 mice (male, 8-week-old, n=6). Mice were grouped when tumor volume reached approximately 100 mm^3, at which time they were treated with anti-human PD-1 (Pembrolizumab, in house) and/or anti-human CCR8 antibodies as indicated. (A) Anti-human PD-1 antibody combined with an anti-human CCR8 antibody (in house) inhibited MC38 tumor growth in B-hPD-1/hPD-L1/hCCR8 mice. (B) Body weight changes during treatment. B-hPD-1/hPD-L1/hCCR8 mice provide a powerful preclinical model for *in vivo* evaluation of anti-human PD-1 and CCR8 antibodies. Values are expressed as mean ± SEM.

CONCLUSIONS

Protein expression analysis:
Human PD-1, PD-L1 and CCR8 proteins were detected in homozygous B-hPD-1/hPD-L1/hCCR8 mice, but not in wild-type mice.

***In vivo* efficacy of anti-human PD-1 and CCR8 antibodies:**
Anti-human PD-1 antibody combined with an anti-human CCR8 antibody controlled B-hPD-L1 MC38 plus tumor growth in B-hPD-1/hPD-L1/hCCR8 mice.